

Theory of the Topological Spin-Seebeck Effect

Nobuyuki Okuma,^{1,*} Massoud Ramezani Masir,² and Allan H. MacDonald²

¹*Department of Physics, University of Tokyo, Hongo 7-3-1, 113-0033, Japan*

²*Department of Physics, University of Texas at Austin, Austin, TX 78712, USA*

(Dated: December 26, 2016)

The spin-Seebeck effect refers to voltage signals induced in metals by thermally driven spin currents in adjacent magnetic systems. We present a theory of the spin-Seebeck signal in the case where the conductor that supports the voltage signal is the topologically-protected two-dimensional surface-state system at the interface between a ferromagnetic insulator (FI) and a topological insulator (TI). Our theory uses a Dirac model for the TI surface-states and assumes Heisenberg exchange coupling between the TI quasiparticles and the FI magnetization. The spin-Seebeck voltage is induced by the TI surface-states scattering off the non-equilibrium magnon population at the surface of the semi-infinite thermally driven FI. Our theory is readily generalized to spin-Seebeck voltages in any two-dimensional conductor that is exchange coupled to the surface of a FI. Surface state carrier-density dependent signal strengths calculated using Bi₂Te₃ and yttrium iron garnet (YIG) materials parameters are consistent with recent experiments.

PACS numbers: 72.20.Pa, 72.25.Mk, 73.20.-r, 75.76.+j

I. INTRODUCTION

The spin-Seebeck effect (SSE),^{1–5} in which the spin-current response to a temperature gradient in a ferromagnet gives rise to a voltage signal in an adjacent metal, has emerged as a central issue of spin caloritronics.^{6,7} In the case of bilayers^{2–5} formed by an insulating ferromagnet and a non-magnetic metal, for example Pt/yttrium iron garnet (YIG), the signal is interpreted^{2–4} as an inverse spin Hall effect (ISHE) voltage associated with conversion between magnon and electron spin currents at the normal-metal/ferromagnetic-insulator (FI) interface. The FI is often modeled as a magnon gas^{8–11}, with classical dynamics described by the stochastic Landau-Lifshitz-Gilbert equation.¹² Adachi *et al.* explained the SSE by a quantum theory with a temperature difference between electrons in the normal metal and magnons in the FI⁸. Semiclassical theories rest on a description of the conversion of the magnon spin current generated by a thermal gradient to the electron spin current^{9–11} at the FI metal interface.

Recently¹³ a spin-Seebeck signal has been measured at the interface between the topological insulator (TI) Sb-doped Bi₂Te₃ and YIG. (See Fig. 1). This experiment provides an example of a SSE voltage signal induced in a two-dimensional conductor that is coupled to the surface of a FI. Since the bulk of the TI does not support a spin current, it is clear that the SSE voltage signal generation mechanism must differ from the ISHE mechanism thought to act in a FI/non-magnetic metal bilayer. SSE experiments are normally interpreted in terms of momentum-averaged quantities such as the total spin current^{9–11}. Because the TI surface-states are coupled to the FI via exchange interactions, the signal must^{13–15} originate from TI surface-state quasiparticles scattering off the non-equilibrium magnon population at the FI surface. As we show, the spin-Seebeck voltage then depends on the full momentum non-equilibrium distribution of

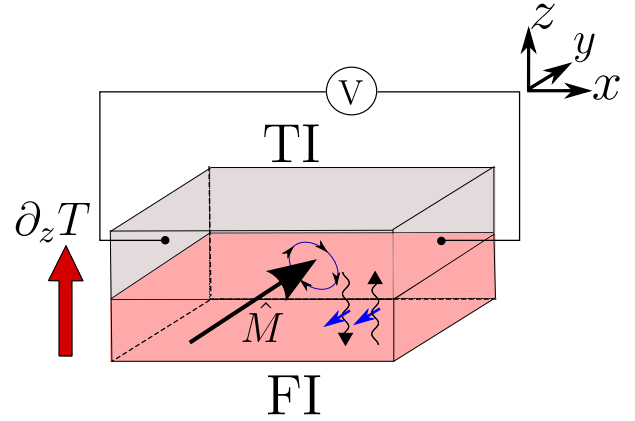


FIG. 1. Schematic illustration of the spin-Seebeck effect in a topological-insulator/ferromagnetic-insulator (FI) bilayer. $\hat{M} \parallel \hat{y}$ indicates the FI ground-state magnetization direction. A finite voltage in the x -direction is generated by a vertical thermal gradient $\partial_z T$.

magnons evaluated at the FI surface, and not just on the non-equilibrium magnon density.

In this paper, we present a theory for the SSE observed in a TI/FI bilayer that is based on the semiclassical transport theory applied to the bulk of the FI and to the TI/FI interface. We show that the non-equilibrium magnon population at the FI surface drives a charge current at the TI surface. By analyzing the magnon and electron Boltzmann equations, we obtain an expression of the electric field induced at the TI surface under open circuit conditions. Our theory can be easily generalized to any two-dimensional conductor at a surface of a magnetic material, *e.g.* to graphene on YIG.

The paper is organized as follows. In Sec. II, we solve the steady-state magnon Boltzmann equation of a semi-infinite FI in the presence of a thermal gradient oriented perpendicular to the surface, assuming specular scatter-

ing of magnons, and extract results for the magnon distribution at the surface. In Sec. III, we consider the spin-momentum-locked Dirac electrons at the TI surface and account for exchange coupling to the FI. Using the non-equilibrium magnon distribution function obtained in Sec. II, we evaluate the non-zero net rate of transitions in the TI surface-state system induced by scattering off the FI's non-equilibrium magnon population and use it to obtain an expression for the electric field induced under open circuit conditions. In Sec. IV, we estimate the typical size of the SSE using materials parameters appropriate for Bi_2Te_3 and YIG and compare our results with experimental data. Some related effects in other hybrid materials are discussed in Sec. V.

II. MAGNON DISTRIBUTION AT THE SURFACE OF A FERROMAGNETIC INSULATOR WITH A PERPENDICULAR TEMPERATURE GRADIENT

In this section, we use the magnon Boltzmann equation with a specular-reflection boundary condition to calculate the magnon distribution function at the surface of a FI with a perpendicular temperature gradient. Henceforth we set $\hbar = k_B = 1$.

A. Model of a ferromagnetic insulator

We consider a FI with magnetization in the y -direction as illustrated in Fig. 1. The low-energy spin excitations of the FI can be described by magnon creation and annihilation operators ($a(\mathbf{x}), a^\dagger(\mathbf{x})$). In the case of a quantum spin-model with spin S_0 degrees-of-freedom on each lattice site, creation and annihilation operators can be introduced by the Holstein-Primakoff transformation: $S^y = S_0 - a^\dagger a$, $S^z + iS^x \simeq \sqrt{2S_0}a$, and $S^z - iS^x \simeq \sqrt{2S_0}a^\dagger$, where S^i is a spin-operator component. In the following, we neglect magnetic anisotropy. The Holstein-Primakoff transformation then leads to a three-dimensional magnon gas with isotropic quadratic dispersion $\omega_{\mathbf{q}} = D|\mathbf{q}|^2$ at long wavelengths. Here D is the spin-stiffness, and \mathbf{q} is the three-dimensional magnon momentum. In terms of magnon operators, the low-energy effective Hamiltonian for the FI is given by

$$H_m = V \int \frac{d^3q}{(2\pi)^3} \omega_{\mathbf{q}} a_{\mathbf{q}}^\dagger a_{\mathbf{q}}, \quad (1)$$

where V is volume. At low energies, this magnon-gas model applies equally well to ferrimagnetic insulators like YIG with a net magnetization due to incomplete cancellation between antiferromagnetically aligned spins.

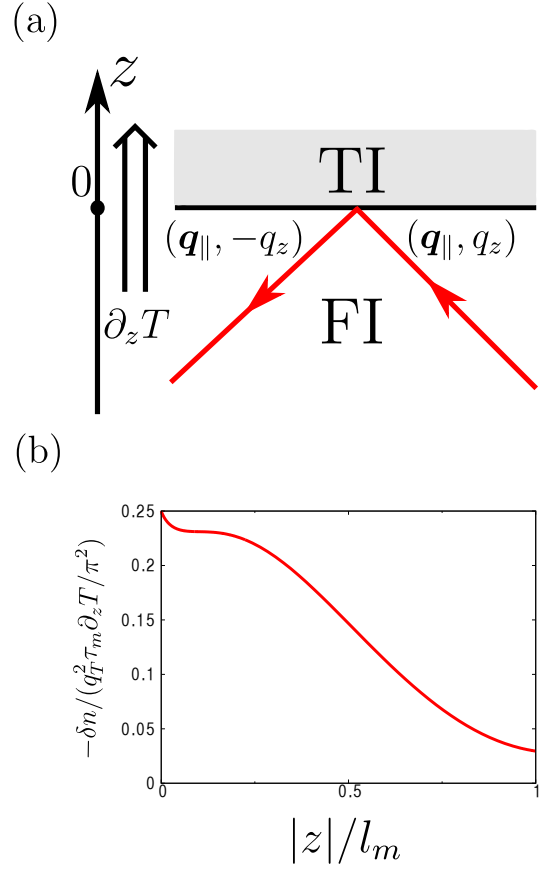


FIG. 2. (a) Schematic illustration of specular reflection of magnons at the FI/TI interface. (b) Total excess magnon population δn as a function of the ratio of the distance from the interface $|z|$ to the magnon mean-free-path l_m .

B. Magnon Boltzmann equation

We now consider the magnon Boltzmann equation in the presence of a thermal gradient:

$$\frac{\partial n_{\mathbf{q}}}{\partial t} + v_{q_z} \partial_z n_{\mathbf{q}} = \left. \frac{\partial n_{\mathbf{q}}}{\partial t} \right|_{\text{scatt}}, \quad (2)$$

where $n_{\mathbf{q}}$ is the momentum-dependent magnon distribution function, $v_{q_z} = \partial_{q_z} \omega_{\mathbf{q}}$ is the magnon velocity, and the right-hand-side term is the scattering term. In the following, we adopt the relaxation time approximation in which the scattering term is given by

$$\left. \frac{\partial n_{\mathbf{q}}}{\partial t} \right|_{\text{scatt}} = -\frac{n_{\mathbf{q}} - n_{\mathbf{q}}^{(0)}(T(z))}{\tau_m}, \quad (3)$$

where $n_{\mathbf{q}}^{(0)} = (\exp(\omega_{\mathbf{q}}/T(z)) - 1)^{-1}$ is the Bose distribution function with local temperature $T(z)$, and τ_m is a magnon relaxation time. The validity of the relaxation time approximation for the scattering term (3) is discussed in Sec. V.

For linear response to a temperature gradient, the Boltzmann equation becomes

$$v_{qz} \left[\partial_z (\delta n_{\mathbf{q}}) + \partial_z T \frac{\partial n_{\mathbf{q}}^{(0)}}{\partial T} \right] = -\frac{\delta n_{\mathbf{q}}}{\tau_m}, \quad (4)$$

where $\delta n_{\mathbf{q}} \equiv n_{\mathbf{q}} - n_{\mathbf{q}}^{(0)}$ is the magnon distribution response. In the following, we solve Eq. (4) assuming specular reflection of magnons at the surface of the FI $z = 0$, *i.e.* we assume that a magnon that approaches the surface from below with momentum $(\mathbf{q}_{\parallel}, q_z)$ is scattered by the interface into a state with momentum $(\mathbf{q}_{\parallel}, -q_z)$ (Fig. 2(a)). This approximation neglects diffuse scattering effects due to surface roughness and does not account for interactions between the magnon system and the TI surface quasiparticles. We show later that the presence of the TI has a negligible influence on the FI magnon distribution. Eq. (4) is an inhomogeneous first-order linear differential equation which we solve by integrating backward along the path followed by the magnon to reach a given position. For magnons at position $z < 0$ that have positive (toward the surface) group velocity, this path does not include reflection whereas for magnons that have negative (away from the surface), the path includes specular reflection at an earlier time. In this way we obtain that for $q_z \geq 0$

$$\begin{aligned} \delta n_{\mathbf{q}_{\parallel}, q_z}(z) &= -\tau_m |v_{qz}| \partial_z T \frac{\partial n_{\mathbf{q}}^{(0)}}{\partial T}, \\ \delta n_{\mathbf{q}_{\parallel}, -q_z}(z) &= \tau_m |v_{qz}| \partial_z T \frac{\partial n_{\mathbf{q}}^{(0)}}{\partial T} \left[1 - 2 \exp \left(-\frac{|z|}{|v_{qz}| \tau_m} \right) \right]. \end{aligned} \quad (5)$$

Note that

$$n_{\mathbf{q}_{\parallel}, q_z}(z=0) = n_{\mathbf{q}_{\parallel}, -q_z}(z=0). \quad (6)$$

Far from the surface, the temperature gradient induces a magnon current, but because of cancellation between $q_z > 0$ and $q_z < 0$ response, it does not change the magnon density. Close to the surface, the cancellation is imperfect. Using Eq. (5), we obtain an expression for the total non-equilibrium magnon density:

$$\begin{aligned} \delta n(z) &\equiv \int_{q_z \geq 0} \frac{d^3 q}{(2\pi)^3} [\delta n_{\mathbf{q}_{\parallel}, q_z} + \delta n_{\mathbf{q}_{\parallel}, -q_z}] \\ &\sim -\frac{\tau_m \partial_z T}{\pi^2} \int_0^1 dt \int_0^{q_T} dq \, q t \exp \left(-\frac{|z|}{2D\tau_m q t} \right). \end{aligned} \quad (7)$$

In the second approximate version of this integrand, we have set $\partial n_{\mathbf{q}}^{(0)}/\partial T \rightarrow 1/\omega_{\mathbf{q}}$ for $|\mathbf{q}| \leq q_T \equiv \sqrt{T/D}$, and to zero for $|\mathbf{q}| > q_T$. Although this approximate expression can be integrated analytically, the result is not particularly transparent. We have plotted the total non-equilibrium magnon distribution obtained by accurately integrating Eq. (7) in Fig. 2(b) where we see that a non-equilibrium magnon population builds up at the surface,

where $l_m \equiv 2Dq_T\tau_m$ is a characteristic magnon mean-free-path. In the following sections, we consider the interaction between the non-equilibrium magnons accumulated at the interface and the electrons on the TI surface-states. We will see that the spin-Seebeck voltage signal depends not only on the total non-equilibrium magnon density, but also on its momentum distribution in relation to the Fermi surface of the TI surface-states.

III. TOPOLOGICAL INSULATOR DIRAC CONE RESPONSE TO NON-EQUILIBRIUM MAGNONS

In this section, we formulate a semiclassical theory of the TI's Dirac cone surface state response to non-equilibrium magnons. Using an electron Boltzmann equation with an electron-magnon-scattering collision term, we are able to obtain an expression of the electric field generated in the TI surface state system by the temperature gradient across the FI.

A. Model of the interface

We model^{14,15} the TI surface-states by a spin-momentum-locked Dirac Hamiltonian:

$$\begin{aligned} H_e &= A \int \frac{d^2 k}{(2\pi)^2} \psi_{\mathbf{k}}^\dagger \hat{\mathcal{H}}_e(\mathbf{k}) \psi_{\mathbf{k}}, \\ \hat{\mathcal{H}}_e(\mathbf{k}) &= v k_x \hat{\sigma}_y - v k_y \hat{\sigma}_x - \mu \hat{1} \\ &= \sum_{\alpha=\pm} \xi_{\mathbf{k}}^\alpha |\mathbf{k}, \alpha\rangle \langle \mathbf{k}, \alpha|, \end{aligned} \quad (8)$$

where A is the system area, (ψ, ψ^\dagger) are two-component creation and annihilation spinors for the surface state electrons, $\mathbf{k} = (k_x, k_y)$ is the two-dimensional electron momentum, v is the Fermi velocity, μ is the chemical potential, and $\hat{\sigma}_i$ are Pauli matrices that act in spin space. In the second line, we define projection operators $|\mathbf{k}, \pm\rangle \langle \mathbf{k}, \pm| = (\hat{1} \pm \mathbf{d}(\mathbf{k}) \cdot \hat{\boldsymbol{\sigma}})/2$ for the upper and lower Dirac bands with energies $\xi_{\mathbf{k}}^\pm = \pm v|\mathbf{k}| - \mu$. Here $\mathbf{d}(\mathbf{k}) = (-\sin \theta_{\mathbf{k}}, \cos \theta_{\mathbf{k}}, 0)$, and $\theta_{\mathbf{k}}$ is the momentum \mathbf{k} orientation angle.

We assume that the surface state quasiparticles are exchange coupled to the surface magnetization of the TI:

$$H_{exc} = -\frac{Ja}{2} \int d^3 x \delta(z) \psi^\dagger(x, y) \hat{\boldsymbol{\sigma}} \psi(x, y) \cdot \mathbf{S}(\mathbf{x}), \quad (9)$$

where a is the lattice constant of the FI, and J characterizes the strength of the exchange coupling. The mean-field coupling between the TI quasiparticles and the y -direction ground state magnetization yields only an irrelevant shift in the k_x -direction in momentum space which has no consequence. For small fluctuations in magnetization direction, the remaining interaction Hamiltonian

can be rewritten as an electron-magnon interaction:

$$\begin{aligned} H_{em} &= -\frac{JaA^3}{2} \sum_{i=x,z} \int \frac{d^2k d^2q_{\parallel}}{(2\pi)^2(2\pi)^2} \psi_{\mathbf{k}}^{\dagger} \hat{\sigma}_i \psi_{\mathbf{k}+\mathbf{q}_{\parallel}} S_{\mathbf{q}_{\parallel}}^i(z=0) \\ &= g \frac{A^3}{a^2} \int \frac{d^2k d^2q_{\parallel}}{(2\pi)^2(2\pi)^2} \psi_{\mathbf{k}}^{\dagger} \hat{\sigma}^+ \psi_{\mathbf{k}+\mathbf{q}_{\parallel}} a_{\mathbf{q}_{\parallel}}^{\dagger}(z=0) + h.c., \end{aligned} \quad (10)$$

where \mathbf{q}_{\parallel} is the in-plane component of the magnon momentum, $g = -\sqrt{2S_0}J/4$, and $\hat{\sigma}^{\pm} = \hat{\sigma}_z \pm i\hat{\sigma}_x$.

B. Electron Boltzmann equation

We concentrate on physics near the Fermi surface and ignore interband scattering. As mentioned in Ref. 13 and explicitly proven in Appendix A, the spin-Seebeck electric field is invariant under a particle-hole transformation $\mu \rightarrow -\mu$ in the simple Dirac model (see for the exact proof). In the following, we therefore assume that

$\mu > 0$, drop band indices and include only the conduction band ($|\mathbf{k}\rangle \equiv |\mathbf{k}, +\rangle$), and $\xi_{\mathbf{k}} \equiv \xi_{\mathbf{k}}^+$, and measure momenta relative to the new Dirac point after the shift produced by the interaction with the ground state magnetization has been applied.

To describe the topological SSE, we consider the linearized Boltzmann equation:

$$\frac{\partial f_{\mathbf{k}}}{\partial t} - e\mathbf{E}^{em} \cdot \mathbf{v}_{\mathbf{k}} \frac{\partial f_{\mathbf{k}}^{(0)}}{\partial \xi_{\mathbf{k}}} = \left. \frac{\partial f_{\mathbf{k}}}{\partial t} \right|_{imp} + \left. \frac{\partial f_{\mathbf{k}}}{\partial t} \right|_{em}, \quad (11)$$

where \mathbf{E}^{em} is the induced electric field, $\mathbf{v}_{\mathbf{k}} = (v_x, v_y) = v(\cos \theta_{\mathbf{k}}, \sin \theta_{\mathbf{k}})$, $f_{\mathbf{k}}$ is the momentum-dependent electron distribution function, and $f_{\mathbf{k}}^{(0)} = (\exp(\xi_{\mathbf{k}}/T) + 1)^{-1}$ is the Fermi distribution function at temperature T . The terms on the right-hand-side terms are the electron-impurity and electron-magnon-scattering collision terms, respectively. The electron-magnon-scattering term can be calculated by using the quantum Fokker-Planck equation,¹⁶ and is given to second order in the electron-magnon interaction by

$$\begin{aligned} \left. \frac{\partial f_{\mathbf{k}}}{\partial t} \right|_{em} &= 2\pi g^2 a^3 \int \frac{d^2q_{\parallel} dq_z}{(2\pi)^3} \\ &\left[|\langle \mathbf{k} + \mathbf{q}_{\parallel} | \hat{\sigma}^- | \mathbf{k} \rangle|^2 \delta(\omega_{\mathbf{q}} + \xi_{\mathbf{k}} - \xi_{\mathbf{k}+\mathbf{q}_{\parallel}}) [(1 - f_{\mathbf{k}}) f_{\mathbf{k}+\mathbf{q}_{\parallel}} (1 + n_{\mathbf{q}_{\parallel}, q_z}(z=0)) - f_{\mathbf{k}} (1 - f_{\mathbf{k}+\mathbf{q}_{\parallel}}) n_{\mathbf{q}_{\parallel}, q_z}(z=0)] \right. \\ &\left. + |\langle \mathbf{k} - \mathbf{q}_{\parallel} | \hat{\sigma}^+ | \mathbf{k} \rangle|^2 \delta(\omega_{\mathbf{q}} - \xi_{\mathbf{k}} + \xi_{\mathbf{k}-\mathbf{q}_{\parallel}}) [(1 - f_{\mathbf{k}}) f_{\mathbf{k}-\mathbf{q}_{\parallel}} n_{\mathbf{q}_{\parallel}, q_z}(z=0) - f_{\mathbf{k}} (1 - f_{\mathbf{k}-\mathbf{q}_{\parallel}}) (1 + n_{\mathbf{q}_{\parallel}, q_z}(z=0))] \right], \end{aligned} \quad (12)$$

where the $|\langle \mathbf{k}' | \hat{\sigma}^{\pm} | \mathbf{k} \rangle|^2$ factors account for the influence of spin-momentum locking in the Dirac cone on the electronic transition probabilities associated with magnon emission and absorption (Fig. 3). This electronic matrix elements can be calculated by observing that the projection operator $|\mathbf{k}\rangle\langle\mathbf{k}| = (\hat{1} + \mathbf{d}(\mathbf{k}) \cdot \hat{\boldsymbol{\sigma}})/2$:

$$\begin{aligned} |\langle \mathbf{k}' | \hat{\sigma}^{\pm} | \mathbf{k} \rangle|^2 &= \text{Tr} [\hat{\sigma}^{\pm} |\mathbf{k}\rangle\langle\mathbf{k}| \hat{\sigma}^{\mp} |\mathbf{k}'\rangle\langle\mathbf{k}'|] \\ &= (1 \mp d^y(\mathbf{k}))(1 \pm d^y(\mathbf{k}')). \end{aligned} \quad (13)$$

The non-equilibrium nature of the SSE is captured by the statistical factors in small square brackets in Eq. (12), which can be further simplified. In linear response we can replace $f_{\mathbf{k}}$ by $f_{\mathbf{k}}^{(0)}$ in the electron-magnon scattering term. Since the right hand side of Eq. (12) is zero by detailed balance, when the magnons are also in equilibrium,

the two square-bracket statistical factors can be replaced by the following two factors:

$$\begin{aligned} (f_{\mathbf{k}+\mathbf{q}_{\parallel}}^{(0)} - f_{\mathbf{k}}^{(0)}) \delta n_{\mathbf{q}_{\parallel}, q_z}(z=0), \\ (f_{\mathbf{k}-\mathbf{q}_{\parallel}}^{(0)} - f_{\mathbf{k}}^{(0)}) \delta n_{\mathbf{q}_{\parallel}, q_z}(z=0), \end{aligned} \quad (14)$$

With this replacement the electron-magnon scattering term is replaced explicitly in terms of the non-equilibrium correction to the magnon distribution function at the interface $\delta n_{\mathbf{q}_{\parallel}, q_z}(z=0)$. Next, the integral over q_z in Eq. (5) can be evaluated using the energy conservation δ -functions,

$$\begin{aligned} \int_{-\infty}^{\infty} dq_z |v_{q_z}| \delta(\omega_{\mathbf{q}} - X) &= 2 \int_0^{\infty} dq_z (2Dq_z) \delta(\omega_{\mathbf{q}} - X), \\ &= 2\Theta(X - D|\mathbf{q}_{\parallel}|^2), \end{aligned} \quad (15)$$

to obtain

$$\left. \frac{\partial f_{\mathbf{k}}}{\partial t} \right|_{em} = g^2 a^3 (-2\tau_m \partial_z T) \int \frac{d^2 q_{\parallel}}{(2\pi)^2} \left[|\langle \mathbf{k} + \mathbf{q}_{\parallel} | \hat{\sigma}^- | \mathbf{k} \rangle|^2 \Theta(\xi_{\mathbf{k}+\mathbf{q}_{\parallel}} - \xi_{\mathbf{k}} - D|\mathbf{q}_{\parallel}|^2) (f_{\mathbf{k}+\mathbf{q}_{\parallel}}^{(0)} - f_{\mathbf{k}}^{(0)}) \frac{\partial n^{(0)}(\xi_{\mathbf{k}+\mathbf{q}_{\parallel}} - \xi_{\mathbf{k}})}{\partial T} \right. \\ \left. + |\langle \mathbf{k} - \mathbf{q}_{\parallel} | \hat{\sigma}^+ | \mathbf{k} \rangle|^2 \Theta(\xi_{\mathbf{k}} - \xi_{\mathbf{k}-\mathbf{q}_{\parallel}} - D|\mathbf{q}_{\parallel}|^2) (f_{\mathbf{k}-\mathbf{q}_{\parallel}}^{(0)} - f_{\mathbf{k}}^{(0)}) \frac{\partial n^{(0)}(\xi_{\mathbf{k}} - \xi_{\mathbf{k}-\mathbf{q}_{\parallel}})}{\partial T} \right]. \quad (16)$$

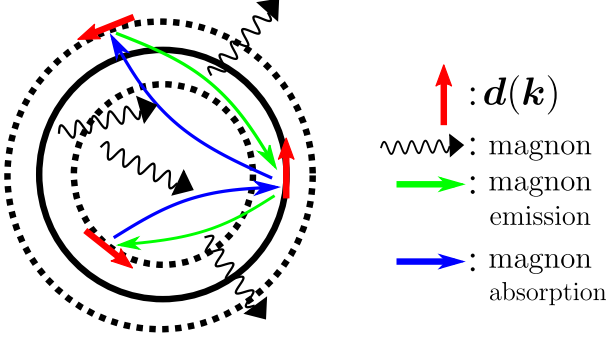


FIG. 3. Schematic illustration of magnon emission and absorption. The solid and dotted circles are constant-energy surfaces for the conduction band and the arrows indicate the importance of spin-momentum locking in the Dirac cone. Magnon emission lowers energy and is accompanied by a $\hat{\sigma}^+$ electronic operator whereas magnon absorption increases energy and is accompanied by a $\hat{\sigma}^-$ electronic operator.

Note that the free-integral over q_z , present because the three-dimensional magnon system is driving a two-dimensional electronic system, replaces the usual Fermi's golden rule δ -function by a step functions.

Since we do not assume any particular property of the TI surface-states in Eq. (16), our theory applies to any single-band two-dimensional electron system that is exchange coupled to the surface magnetism of a ferromagnetic insulator, and is simply generalized to multi-band two-dimensional materials by adding band indices.

C. Induced electric field in the steady-state

We are now in a position to derive an expression for the electric field induced by the electron-magnon interaction in the steady-state. For simplicity, we use a relaxation-time approximation for the electron-impurity collision term in the steady-state electron Boltzmann equation:

$$-e\mathbf{E}^{em} \cdot \mathbf{v}_{\mathbf{k}} \frac{\partial f_{\mathbf{k}}^{(0)}}{\partial \xi_{\mathbf{k}}} = -\frac{\delta f_{\mathbf{k}}}{\tau_e} + \left. \frac{\partial f_{\mathbf{k}}}{\partial t} \right|_{em}, \quad (17)$$

where $\delta f_{\mathbf{k}} = f_{\mathbf{k}} - f_{\mathbf{k}}^{(0)}$, and τ_e is the relaxation time. Since the spin-Seebeck voltage is measured under open circuit conditions, it can be evaluated by finding the electric field

strength at which the electric current vanishes:

$$\int \frac{d^2 k}{(2\pi)^2} \mathbf{v}_{\mathbf{k}} \delta f_{\mathbf{k}} = 0. \quad (18)$$

Using Eqs. (17) and (18), we find that

$$E_i^{em} = \left[\int \frac{d^2 k}{(2\pi)^2} v_i \left. \frac{\partial f_{\mathbf{k}}}{\partial t} \right|_{em} \right] / \left[-e \int \frac{d^2 k}{(2\pi)^2} v_i^2 \frac{\partial f_{\mathbf{k}}^{(0)}}{\partial \xi_{\mathbf{k}}} \right]. \quad (19)$$

In deriving Eq. (19), we have appealed to isotropy in asserting that $\int d^2 k v_x v_y = 0$. Note that E_i^{em} is independent of the electron-disorder scattering time τ_e .

In the topological SSE for magnetization in the y -direction, the induced electric field is in the x -direction: $\mathbf{E}^{em} = (E_x^{em}, 0)$. To see this, we rewrite Eq. (13) as

$$|\langle \mathbf{k}' | \hat{\sigma}^{\pm} | \mathbf{k} \rangle|^2 = \pm \cos \theta_{\mathbf{k}} (\cos \Delta \theta_{\mathbf{k}, \mathbf{k}'} - 1) \\ - \sin \theta_{\mathbf{k}} (\cos \theta_{\mathbf{k}} \mp 1) \sin \Delta \theta_{\mathbf{k}, \mathbf{k}'} \\ + (1 - \cos^2 \theta_{\mathbf{k}} \cos \Delta \theta_{\mathbf{k}, \mathbf{k}'}), \quad (20)$$

where $\Delta \theta_{\mathbf{k}, \mathbf{k}'} \equiv \theta_{\mathbf{k}} - \theta_{\mathbf{k}'}$. The second line on the right hand side of Eq. (20) does not contribute to Eq. (16) because the other factors in the integrand are even function of $\Delta \theta_{\mathbf{k}, \mathbf{k}'}$. The term on the third line does not contribute to the numerator Eq. (19) because its contribution to the integrand is odd in $\sin \theta_{\mathbf{k}}$ or $\cos \theta_{\mathbf{k}}$. Similarly the first line contributes to E_x^{em} ($v_x \propto \cos \theta_{\mathbf{k}}$), but not to E_y^{em} ($v_y \propto \sin \theta_{\mathbf{k}}$). The electric-field direction predicted by our theory is consistent with the experimental result¹³.

In the following sections, we retain only the first line on the right hand side of Eq. (20) since the other terms do not contribute to the final result. For notational convenience, we therefore rewrite Eq. (16) as

$$\left. \frac{\partial f_{\mathbf{k}}}{\partial t} \right|_{em} = g^2 a^3 (-2\tau_m \partial_z T) \cos \theta_{\mathbf{k}} A(vk), \quad (21)$$

where A is a $\theta_{\mathbf{k}}$ -independent function.

IV. NUMERICAL RESULTS

To compare our theory with experiment¹³, we compute the integrals in the numerator and denominator of Eq. (17). For numerical estimates, we use $v = 3.0 \times 10^5$ m/s for the surface state Dirac velocity of Bi_2Te_3 ¹⁷ and $D = 5.0 \times 10^{-21}$ eV m² for the spin-stiffness of YIG^{18,19}.

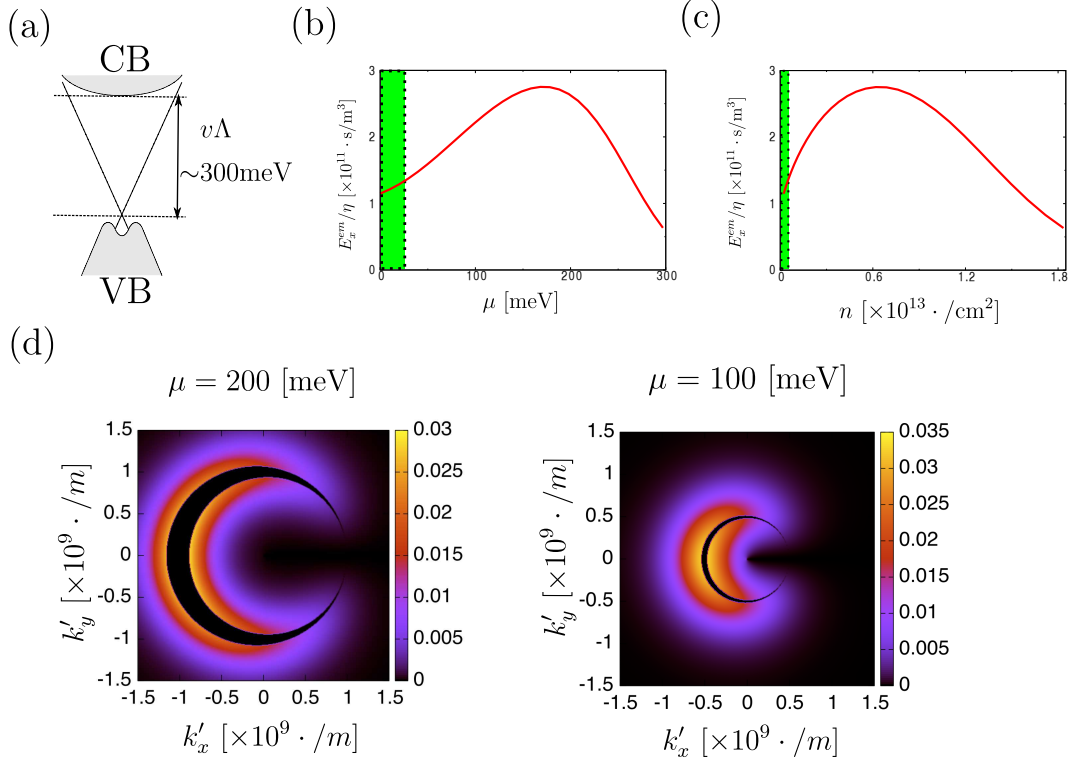


FIG. 4. (a) Schematic illustration of the band structure of a Bi_2Te_3 film. The shaded regions labelled VB and CB are the bulk valence conduction bands, respectively. The surface state Dirac point is much closer to the valence band than to the conduction band. The thermally electric field at $T = 300 \text{ K}$ is plotted in (b) vs. chemical potential and in (c) vs. electron density. In the green region ($\mu \leq T$), the results are not accurate since we neglect the inter-band effect. (d) The integrand of Eq. (16) in arbitrary units for $\mathbf{k} = (k_F, 0)$ as a function of \mathbf{k}' for chemical potential $\mu = 100$ and 200 meV relative to the Dirac point. The electron-magnon interaction vertex tends to be strongest for transitions between electronic states with opposite momentum.

The momentum cutoff Λ of the TI surface-states is fixed by setting $v\Lambda$ equal to the bulk band gap¹⁷ $\sim 300 \text{ meV}$, which yields $\Lambda \sim 1.5 \times 10^9 \text{ /m}$. (See Fig. 4(a)). The spin-Seebeck signal is proportional to $\eta \equiv 2g^2 a^3 \tau_m \partial_z T / e$.

A. Trend vs. carrier density

Since the motivating experiment is performed at room temperature, we first set $T = 300 \text{ K}$ and examine in Fig. 4(b) the dependence of the spin-Seebeck signal on the position of the Fermi level. We find a non-monotonic dependence that is illustrated by plotting the thermally induced electric field E_x^{em} as a function of the chemical potential μ in Fig. 4(b) and as a function of electron density $n \equiv \int d^2k / (2\pi)^2 f_k^{(0)}$ in Fig. 4(c). The non-monotonic behavior arises from the momentum distribution of the non-equilibrium magnons combined with the increase with μ in the electronic density-of-states, which enhances the phase space available for electron-magnon scattering. To illustrate this anomalous behavior, we plot in Fig. 4(d) the integrand of Eq. (16) for fixed $\mathbf{k} = (k_F, 0)$, where $k_F = \mu/v$ is the Fermi momentum, as a function of $\mathbf{k}' = \mathbf{k} \pm \mathbf{q}$. Because the

electron-magnon interaction vertex reverses spins relative to the magnetization direction, the integrand tends to be stronger for transitions between electronic states with opposite momentum directions. At the larger chemical potential ($\mu = 200 \text{ meV}$) value, large angle scatterings is suppressed due to the lack of available magnons which is captured by the step functions and the other part of the integrand. Suppression by the step function is weaker at smaller chemical potential ($\mu = 100 \text{ meV}$). Our use of a momentum cutoff, which crudely captures the less stark spin-momentum coupling in bulk and higher energy surface state bands, also compete with the density-of-states effect to produce a maximum spin-Seebeck signal at a finite chemical potential. Because we neglect the role of valence band states, our calculations are not accurate at very small carrier densities ($\mu \lesssim T$). In our calculations E_x^{em} has its maximum value at $n = 6 \times 10^{12} \text{ /cm}^2$. In experiment, the electric field at $n = 4 \times 10^{12} \text{ /cm}^2$ is found to be ~ 50 times greater than that at $n = 2 \times 10^{13} \text{ /cm}^2$. Our numerical result explains the electric field enhancement at relatively small electron densities, although our simplified model does not achieve quantitative agreement.

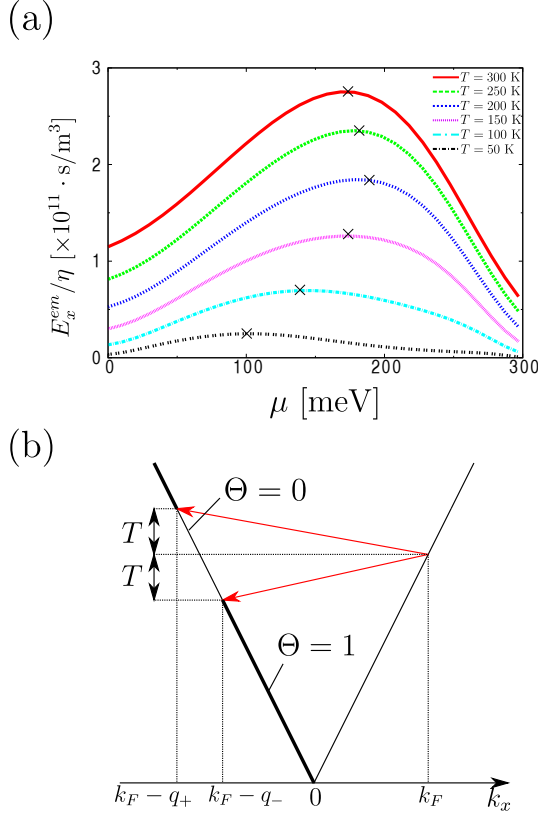


FIG. 5. (a) Spin-Seebeck electric field E_x^{em} as a function of μ for various temperatures. The cross marks denote the largest electric field points for each temperature. (b) Schematic illustration of electron-magnon backscattering $\mathbf{k} = (k_F, 0) \rightarrow \mathbf{k}' = (-|\mathbf{k}'|, 0)$ at $\mu = \mu_{max}^{est}$.

B. Order of magnitude estimate

In order to estimate the numerical size of the spin-Seebeck signal at room temperature, we use the following typical values for YIG¹¹: $S_0 \sim 10$ and $a \sim 10^{-9}\text{m}$. Assuming that the dominant magnon relaxation mechanism is related to Gilbert damping of the macroscopic magnetization at room temperature (see Sec. V A), we use $\tau_m \sim \hbar/\alpha_G k_B T \sim 10^{-9} \text{ s}^{11,20,21}$, where $\alpha_G \sim 10^{-4}$. Finally we set the interface exchange coupling to $J \sim 1 \text{ meV}$, the same order as for a Pt/YIG interface. From Fig. 4(b), the maximum value of E_x^{em}/η at room temperature is $\sim 3 \times 10^{11} \text{ s/m}^3$. Using the above values to estimate η , we obtain $E_x^{em} \sim 0.9 \text{ V/m}$ for $\partial_z T \sim 5 \times 10^3 \text{ K/m}$, which is of the same order of magnitude as the experimental value of $\sim 0.2 \text{ V/m}$.

C. Temperature dependence of induced electric field

The μ -dependence of E_x^{em} is plotted for various temperatures in Fig. 5(a). The overall trend is that E_x^{em}

increases with temperature because of the increase in magnon population. The chemical potential at which E_x^{em} reaches its maximum μ_{max} , decreases with decreasing temperature for $T \lesssim 200 \text{ K}$. μ_{max} can be roughly estimated by considering back-scattering contributions, e.g. $\mathbf{k} = (k_F, 0) \rightarrow \mathbf{k}' = (-|\mathbf{k}'|, 0)$. For each k_F , we define q_{\pm} such that

$$Dq_{\pm}^2 = \pm(v(q_{\pm} - k_F) - vk_F). \quad (22)$$

Because of the magnon contribution to the final state energy, the step functions in the integrand of Eq. (16) both vanish for $q_- - k_F < |\mathbf{k}'| < q_+ - k_F$ (See Fig. 5(b)). For $|q_{\pm} - 2k_F| \ll k_F$, $q_{\pm} \simeq 2k_F \pm 4Dk_F^2/v$. In this approximation, the step functions are zero for

$$k_F - \frac{4Dk_F^2}{v} \lesssim |\mathbf{k}'| \lesssim k_F + \frac{4Dk_F^2}{v}. \quad (23)$$

Since the magnon statistical factors have large values for $k_F - T/v \lesssim |\mathbf{k}'| \lesssim k_F + T/v$, the overlap with the step functions is large when $k_F < \sqrt{T/4D}$. Roughly speaking, μ_{max} is expected to be given by

$$\mu_{max}^{est} = \frac{v}{2} \sqrt{\frac{T}{D}}. \quad (24)$$

According to Eq. (24), $\mu_{max}^{est} = 100, 140, 170, 200, 220$, and 240 meV for $T = 50, 100, 150, 200, 250$, and 300 K , respectively, in good agreement with the more accurate values in Fig. 5(a) for $T \lesssim 200 \text{ K}$. Eq. (24) cannot explain the maximum values for $T = 250$ and 300 K , where μ_{max}^{est} is close to $v\Lambda \sim 300 \text{ meV}$, because these considerations do not account for the Dirac surface state cut-off.

V. DISCUSSIONS

A. The magnon collision integral

We now return to discuss our use of a relaxation time approximation in the magnon Boltzmann equation (Eq. (3)). At room temperature, magnon-phonon-scattering processes dominate magnon relaxation. Our assumption of characteristic time over which any un-driven non-equilibrium magnon population will approach equilibrium is consistent with stochastic Landau-Lifshitz-Gilbert equations¹² in which the magnetization relaxation appears in the Gilbert damping term. (See Sec. IV B.) It is nevertheless important to distinguish the roles of processes that conserve magnon number, for example processes in which a magnon and a phonon exchange energy and momentum, from processes that do not conserve magnon-number, for example ones in which magnons are converted into phonons and vice versa. If the former processes are strongly dominant, a possibility proposed by Cornelissen *et al.*¹¹, the non-equilibrium magnon distribution can assume a different form characterized by a

local chemical potential and this might have a quantitative influence on the topological SSE. The magnon-phonon conversion processes that we have in mind in using the relaxation time approximation, correspond to changes in the ground state magnetization configuration, in response to changes in the lattice. Although they have not been thoroughly explored either theoretically or experimentally, as far as we are aware, they are certainly present at all magnon wavelengths.

Another important issue in our theory is the influence of electron-magnon scattering at the surface on the magnon distribution function, which we have assumed is negligible. To justify this approximation, we now compare the rate of spin injection due to magnon-electron scattering with the total magnon relaxation rate.

The spin injection rate is given by

$$\left. \frac{\partial s^y}{\partial t} \right|_{em} \equiv \int \frac{d^2 k}{(2\pi)^2} \frac{d^y(\mathbf{k})}{2} \left. \frac{\partial f_{\mathbf{k}}}{\partial t} \right|_{em}. \quad (25)$$

For an order-of-magnitude estimate, we use the following approximations:

$$\Theta(|\xi_{\mathbf{k}'} - \xi_{\mathbf{k}}| - D|\mathbf{k} - \mathbf{k}'|^2) \sim 1, \quad (26)$$

$$k_F - \frac{T}{v} \lesssim |\mathbf{k}'| \lesssim k_F + \frac{T}{v}, \quad (27)$$

$$(f_{\mathbf{k}'}^{(0)} - f_{\mathbf{k}}^{(0)}) \frac{\partial n^{(0)}(\xi_{\mathbf{k}'} - \xi_{\mathbf{k}})}{\partial T} \sim \frac{\partial f_{\mathbf{k}}^{(0)}}{\partial \xi_{\mathbf{k}}}. \quad (28)$$

Using Eqs. (26), (27), (28), and $\partial f_{\mathbf{k}}^{(0)} / \partial \xi_{\mathbf{k}} \sim -\delta(\xi_{\mathbf{k}})$, we can rewrite Eqs. (16) and (25) as

$$\left. \frac{\partial f_{\mathbf{k}}}{\partial t} \right|_{em} \sim \frac{8\pi g^2 a^3 k_F (\tau_m T \partial_z T)}{v} \delta(\xi_{\mathbf{k}}) \cos \theta_{\mathbf{k}}, \quad (29)$$

$$\left. \frac{\partial s^y}{\partial t} \right|_{em} \sim \frac{g^2 a^3 k_F^2 (\tau_m T \partial_z T)}{v^2}. \quad (30)$$

In comparison, the total magnon relaxation rate is given by

$$\begin{aligned} & \int_{-\infty}^0 dz \frac{\delta n(z)}{\tau_m} \\ & \sim -\frac{\partial_z T}{\pi^2} \int_{-\infty}^0 dz \int_0^1 dt \int_0^{qT} dq \, qt \exp\left(-\frac{|z|}{2D\tau_m qt}\right) \\ & = -\frac{2qT(\tau_m T \partial_z T)}{9\pi^2}, \end{aligned} \quad (31)$$

where we have used Eq. (7) in the second line. Thus, the ratio of the spin injection rate to the total magnon relaxation rate is approximately given by

$$\left. \frac{\partial s^y}{\partial t} \right|_{em} \bigg/ \left| \int_{-\infty}^0 dz \frac{\delta n(z)}{\tau_m} \right| \sim \frac{9\pi^2 g^2 a^3 k_F^2}{2v^2 qT}. \quad (32)$$

The value of the right hand side of Eq. (32) is $\sim 10^{-3}$ for $k_F, qT \sim 10^9$ /m. It follows that the influence of the TI on the magnon distribution in the FI is indeed negligible.

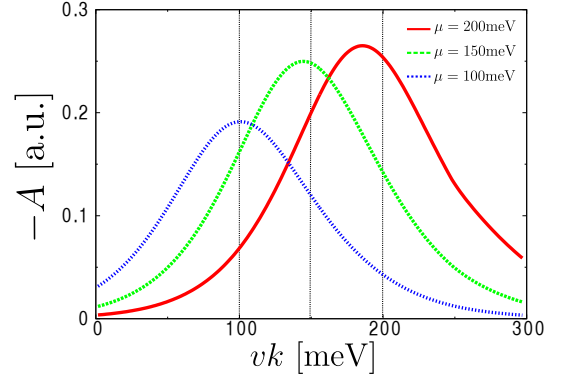


FIG. 6. Energy dependence of the factor A which captures the energy dependence of the Dirac state population response at a given orientation, as a function of vk for several μ values. These results were calculated at room temperature.

B. Corrections to our simplified model

Although our theory explains the topological SSE qualitatively, estimating the correct order of magnitude of the effect and its carrier-density dependence, it does overestimate E_x^{em} in comparison to experiment, especially for large μ . There are mainly two possible reasons. First, both the magnitude and surface-state energy dependence of the exchange-coupling J is uncertain. Second, the surface state in experimentally realized topological insulators are not very accurately described by the simple Dirac electron model. The leading correction²² in Bi_2Te_3 is a hexagonal warping^{24,31} correction:

$$\hat{\mathcal{H}}(\mathbf{k}) \propto (k_x^3 - 3k_x k_y^2) \hat{\sigma}_z, \quad (33)$$

This term implies that $\mathbf{d}(\mathbf{k})$ has a large out-of-plane component for large chemical potentials, which would have the effect of reducing the SSE strength.

C. Thermal gradient generation in x -direction

Since the origin of the electron-magnon scattering term is a temperature gradient, we expect that energy currents will also flow in the topological insulator. In Fig. 6, we plot $A(vk)$ for various chemical potentials. Because $A(vk)$ is an asymmetric function with respect to $vk = \mu$, it follows that electron-magnon scattering drives not only electrical signal but also heat flow. We therefore predict that the $\partial_z T$, applied temperature gradient of the experimental spin-Seebeck geometry, will induce an x -direction temperature gradient $\partial_x T$.

D. SSE in a magnetically doped TI

We now generalize our discussion to magnetically-doped TIs like Cr-doped $(\text{Bi Sb})_2\text{Te}_3$ ²⁵⁻²⁸, Cr-doped

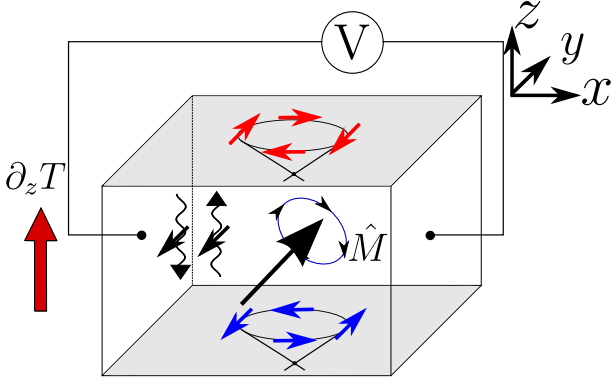


FIG. 7. Schematic illustration of the SSE in a magnetically doped TI thin film.

Bi_2Se_3 ²⁹, and Mn-doped $\text{Bi}_2(\text{Te Se})_3$ ^{30,31}. The anomalous Hall effect in these systems demonstrates robust magnetic order, at least at very low temperatures. Under these conditions a magnetic TI under a vertical temperature gradient (Fig. 7) can be described by a model similar to that discussed elsewhere in this paper. If the film is uniformly magnetized, the two surface state systems will be coupled to the same magnon gas. Because the effective Hamiltonians of the top and bottom surface states have different chiralities,

$$\hat{\mathcal{H}}^{\text{top(bottom)}}(\mathbf{k}) = \pm [-vk_x\hat{\sigma}_y + vk_y\hat{\sigma}_x] - \mu\hat{1}, \quad (34)$$

where top (bottom) corresponds to $+$ ($-$), and the signs of the magnon accumulation at two surfaces are opposite, the charge currents generated at top and bottom surfaces will have the same sign. We therefore predict that a transverse voltage will be induced by a vertical temperature gradient in magnetically doped TI thin films.

ACKNOWLEDGMENTS

The authors acknowledge helpful interactions with Z. Jiang, C. Z. Chang, J. S. Moodera and J. Shi. This work was performed as part of the SHINES, an Energy Frontier Research Center funded by the U.S. Department of Energy, Office of Science, Basic Energy Sciences under Award #SC0012670. N. O. is supported by the Japan Society for the Promotion of Science (JSPS) through Program for Leading Graduate Schools (MERIT). N. O. is also supported by JSPS KAKENHI (Grants No. 16J07110).

Appendix A: Dirac-spinor particle-hole transformation

We prove here that for an ideal symmetric Dirac cone, the thermally induced electric field is unchanged under

$\mu \rightarrow -\mu$. For convenience, we introduce the hole Dirac spinors (ϕ, ϕ^\dagger) defined in terms of (ψ, ψ^\dagger) as:

$$\begin{aligned} \phi_{\mathbf{k}} &= \hat{\sigma}_y \psi_{-\mathbf{k}}^\dagger, \\ \phi_{\mathbf{k}}^\dagger &= \psi_{-\mathbf{k}} \hat{\sigma}_y, \end{aligned} \quad (A1)$$

or equivalently,

$$\begin{aligned} \phi(\mathbf{x}) &= \hat{\sigma}_y \psi^\dagger(\mathbf{x}), \\ \phi^\dagger(\mathbf{x}) &= \psi(\mathbf{x}) \hat{\sigma}_y. \end{aligned} \quad (A2)$$

This particle-hole transformation is defined such that the matrix representation of spin density operator is unchanged:

$$\mathbf{s}(x) \equiv \psi^\dagger(x) \left[\frac{\hat{\boldsymbol{\sigma}}}{2} \right] \psi(x) = \phi^\dagger(x) \left[\frac{\hat{\boldsymbol{\sigma}}}{2} \right] \phi(x). \quad (A3)$$

The electron Dirac Hamiltonian (8) can be rewritten in terms of (ϕ, ϕ^\dagger) as

$$\begin{aligned} H_e &= \int \frac{d^2k}{(2\pi)^2} \psi_{\mathbf{k}}^\dagger \hat{\mathcal{H}}_e(\mathbf{k}) \psi_{\mathbf{k}} \\ &= (\text{Const.}) + \int \frac{d^2k}{(2\pi)^2} \psi_{-\mathbf{k},i} [-\hat{\mathcal{H}}_e^*(-\mathbf{k})]_{i,j} \psi_{-\mathbf{k},j}^\dagger \\ &= (\text{Const.}) + \int \frac{d^2k}{(2\pi)^2} \phi_{\mathbf{k}}^\dagger [-\hat{\sigma}_y \hat{\mathcal{H}}_e^*(-\mathbf{k}) \hat{\sigma}_y] \phi_{\mathbf{k}} \\ &= (\text{Const.}) + \int \frac{d^2k}{(2\pi)^2} \phi_{\mathbf{k}}^\dagger [-(vk_x \hat{\sigma}_y - vk_y \hat{\sigma}_x) + \mu \hat{1}] \phi_{\mathbf{k}}. \end{aligned} \quad (A4)$$

Eq. (A4) shows that the particle-hole transformation changes the sign of μ and the chirality of the Dirac Hamiltonian. The form of the electron-magnon Hamiltonian (10), on the other hand, does not change under the particle-hole transformation:

$$H_{em} = g \int \frac{d^2k d^2q_{\parallel}}{(2\pi)^2 (2\pi)^2} \phi_{\mathbf{k}}^\dagger \hat{\sigma}^+ \phi_{\mathbf{k}+\mathbf{q}_{\parallel}} a_{\mathbf{q}_{\parallel}}^\dagger (z=0) + h.c., \quad (A5)$$

since the magnon operators couple not to the charge density but to the hole spin density that has the same matrix representation as the electron spin density.

In the following, we consider the electron Dirac Hamiltonian with $\mu = -|\mu_0|$. This Hamiltonian is equivalent to the hole Dirac Hamiltonian with $\mu = |\mu_0|$. The scattering term (16) for this hole Dirac Hamiltonian has the same magnitude but the opposite sign as that for the electron Dirac Hamiltonian with $\mu = |\mu_0|$ due to its opposite chirality, while the definition of the electric field (19) for the hole Dirac Hamiltonian has the opposite sign as that for the electron Dirac Hamiltonian due to its opposite charge. Thus, the induced electric field for the hole Dirac Hamiltonian with $\mu = |\mu_0|$ is the same as that for the electron Dirac Hamiltonian with $\mu = |\mu_0|$, or equivalently, the induced electric field for the electron Dirac Hamiltonian is unchanged as $\mu_0 \rightarrow -\mu_0$.

-
- * okuma@hosi.phys.s.u-tokyo.ac.jp
- ¹ K. Uchida, S. Takahashi, K. Harii, J. Ieda, W. Koshibae, K. Ando, S. Maekawa, and E. Saitoh, *Nature* **455**, 778 (2008).
 - ² K. Uchida, J. Xiao, H. Adachi, J. Ohe, S. Takahashi, J. Ieda, T. Ota, Y. Kajiwara, H. Umezawa, H. Kawai, G. E. W. Bauer, S. Maekawa, and E. Saitoh, *Nature Mater.* **9**, 894 (2010).
 - ³ K. Uchida, H. Adachi, T. Ota, H. Nakayama, S. Maekawa, and E. Saitoh, *Appl. Phys. Lett.* **97**, 172505 (2010).
 - ⁴ T. Kikkawa, K. Uchida, Y. Shiomi, Z. Qiu, D. Hou, D. Tian, H. Nakayama, X.-F. Jin, and E. Saitoh, *Phys. Rev. Lett.* **110**, 067207 (2013).
 - ⁵ D. Qu, S. Y. Huang, Jun Hu, Ruqian Wu, and C. L. Chien, *Phys. Rev. Lett.* **110**, 067206 (2013).
 - ⁶ G. E. W. Bauer, A. H. MacDonald, and S. Maekawa (Eds), *Spin Caloritronics, Special Issue of Solid State Communications* (Elsevier, 2010).
 - ⁷ G. E. W. Bauer, E. Saitoh, and B. J. van Wees, *Nature materials* **11**, 391 (2012).
 - ⁸ H. Adachi, K. Uchida, E. Saitoh, and S. Maekawa, *Rep. Prog. Phys.* **76**, 036501 (2013).
 - ⁹ Steven S. -L. Zhang and S. Zhang, *Phys. Rev. B* **86**, 214424 (2012).
 - ¹⁰ Steven S. -L. Zhang and S. Zhang, *Phys. Rev. Lett.* **109**, 096603 (2012).
 - ¹¹ L. J. Cornelissen, K. J. H. Peters, G. E. W. Bauer, R. A. Duine, and B. J. van Wees, *Phys. Rev. B* **94**, 014412 (2016).
 - ¹² S. Hoffman, K. Sato, Y. Tserkovnyak, *Phys. Rev. B* **88**, 064408 (2013).
 - ¹³ Z. Jiang, C. Z. Chang, M. Ramezani Masir, C. Tang, Y. Xu, J. S. Moodera, A. H. MacDonald, and J. Shi, *Nat. Commun.* **7**, 11458 (2016).
 - ¹⁴ M. Z. Hasan and C. L. Kane, *Rev. Mod. Phys.* **82**, 3045 (2010).
 - ¹⁵ X.-L. Qi and S.-C. Zhang, *Rev. Mod. Phys.* **83**, 1057 (2011).
 - ¹⁶ D. W. Snoke, *Solid State Physics : Essential Concepts* (Pearson/Addison-Wesley, San Francisco, 2009).
 - ¹⁷ J. Zhang, C.-Z. Chang, Z. Zhang, J. Wen, X. Feng, K. Li, M. Liu, K. He, L. Wang, X. Chen, Q.-K. Xue, X. Ma, and Y. Wang, *Nat. Commun.* **2**, 574 (2011).
 - ¹⁸ S. S. Shinozaki, *Phys. Rev.* **122**, 388 (1961).
 - ¹⁹ C. M. Srivastava and R. Aiyar, *J. Phys. C* **20**, 1119 (1987).
 - ²⁰ T. L. Gilbert, *IEEE Trans. Magn.* **40**, 3443 (2004).
 - ²¹ S. A. Bender, R. A. Duine, A. Brataas, and Y. Tserkovnyak, *Phys. Rev. B* **90**, 094409 (2014).
 - ²² L. Fu, *Phys. Rev. Lett.* **103**, 266801 (2009).
 - ²³ Y. L. Chen, J. G. Analytis, J.-H. Chu, Z. K. Liu, S.-K. Mo, X. L. Qi, H. J. Zhang, D. H. Lu, X. Dai, Z. Fang, S. C. Zhang, I. R. Fisher, Z. Hussain, Z.-X. Shen, *Science* **325**, 178 (2009).
 - ²⁴ D. Hsieh, Y. Xia, D. Qian, L. Wray, J. H. Dil, F. Meier, J. Osterwalder, L. Patthey, J. G. Checkelsky, N. P. Ong, A. V. Fedorov, H. Lin, A. Bansil, D. Grauer, Y. S. Hor, R. J. Cava, and M. Z. Hasan, *Nature* **460**, 1101 (2009).
 - ²⁵ X. Kou, L. He, M. Lang, Y. Fan, K. Wong, Y. Jiang, T. Nie, W. Jiang, P. Upadhyaya, Z. Xing, Y. Wang, F. Xiu, R. N. Schwartz, and K. L. Wang, *Nano Letters* **13**, 4587 (2013).
 - ²⁶ C.-Z. Chang, J. Zhang, M. Liu, Z. Zhang, X. Feng, K. Li, L.-L. Wang, X. Chen, X. Dai, Z. Fang, X.-L. Qi, S.-C. Zhang, Y. Wang, K. He, X.-C. Ma, and Q.-K. Xue, *Adv. Mater.* **25**, 1065 (2013).
 - ²⁷ C.-Z. Chang, J. Zhang, X. Feng, J. Shen, Z. Zhang, M. Guo, K. Li, Y. Ou, P. Wei, L.-L. Wang, Z.-Q. Ji, Y. Feng, S. Ji, X. Chen, J. Jia, X. Dai, Z. Fang, S.-C. Zhang, K. He, Y. Wang, L. Lu, X.-C. Ma, and Q.-K. Xue, *Science* **340**, 167 (2013).
 - ²⁸ Y. Fan, P. Upadhyaya, X. Kou, M. Lang, S. Takei, Z. Wang, J. Tang, L. He, L.-T. Chang, M. Montazeri, G. Yu, W. Jiang, T. Nie, R. N. Schwartz, Y. Tserkovnyak, and K. L. Wang, *Nature Mater.* **13**, 699 (2014).
 - ²⁹ X. F. Kou, W. J. Jiang, M. R. Lang, F. X. Xiu, L. He, Y. Wang, Y. Wang, X. X. Yu, A. V. Fedorov, P. Zhang, and K. L. Wang, *J. Appl. Phys.* **112**, 063912 (2012).
 - ³⁰ J. G. Checkelsky, Jianting Ye, Yoshinori Onose, Yoshihiro Iwasa and Yoshinori Tokura, *Nature Phys.* **8**, 729(2012).
 - ³¹ Y. L. Chen, J. H. Chu, J. G. Analytis, Z. K. Liu, K. Igarashi, H. H. Kuo, X. L. Qi, S. K. Mo, R. G. Moore, D. H. Lu, et al., *Science* **329**, 659 (2010).